



Effects of different WAAM current deposition modes on the mechanical properties of AISI H13 tool steel

William Hackenhaar¹ · José A. E. Mazzaferro¹ · Cintia C. P. Mazzaferro¹ · Niccolò Grossi² · Gianni Campatelli²

Received: 27 October 2021 / Accepted: 30 June 2022 / Published online: 8 July 2022
© International Institute of Welding 2022

Abstract

In this work, AISI H13 tool steel build-ups were produced through wire arc additive manufacturing (WAAM). The cold metal transfer (CMT), low spatter control (LSC) and pulsed synergic (PS) current deposition modes were compared. Similar deposition strategy was employed in order to attempt to evaluate the influence of energy input on geometrical and mechanical properties of the deposits. To evaluate the mechanical properties of the deposits, hardness and tensile tests were carried out. Microstructures were analysed in optical microscope. As a result of the intrinsic characteristics of each current waveform and adjustments of the heat source used to perform the deposits, the heat input value was similar for CMT and PS mode and lower for the LSC mode. The CMT deposit was the tallest and widest. Temperatures were higher using the PS deposition mode. The hardness values for all deposits were higher than the usual ones for this tool steel. The microstructure was composed by hard phases, and the precipitates at grain boundaries were responsible for the brittle fracture observed in tensile specimens.

Keywords Wire arc additive manufacturing · Mechanical properties · AISI H13 Steel · Current waveform · WAAM deposition mode

1 Introduction

Additive manufacturing (AM) is a technology that allows the production and repair of products with complex geometry and made of difficult-to-cut materials. From the economic perspective, the application of AM technologies is very beneficial when applied to the production of small batches or when a “mass customization” of product is required [1]. Lately, AM development has been strongly supported by the transition to the Industry 4.0 paradigm [2]. Also, the last COVID-19 crisis showed the potential for AM technologies when an urgent need for spare or new parts are required [3]. The most common AM technologies for metals are based on powder-bed that are able to create very complex shape products but are characterised by low productivity and dimension limitations. Alternative approaches that do not require

the use of a powder bed have been developed, known as direct energy deposition (DED) methods. These use different strategies to melt a metal feedstock, mainly powder or wire, and create a bead of fused metal on a substrate. The main approaches use laser beam, electron beam and electrical arc as deposition sources. In general, the use of powder allows to achieve better accuracy at a lower deposition rate, while the use of wire is a faster but less accurate process [4]. The advantage of DED approaches is suitable not only for the production of brand-new components but also for repairing high-cost parts, like turbine blades or stamping dies.

In this paper, wire arc additive manufacturing (WAAM) is used to build-up a model component with deposition of successive layers of AISI H13 steel, often used in the toolmaking and die sector. WAAM is basically a 3D welding process based on fusion Gas Metal Arc Welding (GMAW) that uses a metal wire electrode and an electrical arc to create a deposition bead. The main advantages are the possibility to create very large parts like the ship propeller made by RAM-LAB [5], with a very high deposition rate that could reach more than 10 kg per hour using different metallic alloys as steel, aluminium-based, titanium-based and others [6]. Typically, the resulting shape is affected by a relevant waviness of the surfaces, so often it is required a finishing step on a

✉ William Hackenhaar
williamhackenhaar@gmail.com

¹ Welding & Related Techniques Laboratory, Federal University of Rio Grande Do Sul UFRGS/PROMECA, Porto Alegre, RS, Brazil

² Department of Industrial Engineering, University of Firenze, Via di Santa Marta 3, 50139 Florence, Italy

machine tool to complete the production cycle. WAAM is interesting also due to the easy integration on a numerical control machine tool to create an hybrid additive-subtractive machine, a solution already available from most prominent machine tool manufacturers [7].

Since WAAM is often used to produce thin-walled structures by building-up successive layers of metal, the heat accumulation in the workpiece is one of the main issues of this approach. Therefore, advanced solutions to lower the heat input of the deposition process are adopted both for the current/voltage waveform and for the wire feeding. An example is the cold metal transfer (CMT) mode that introduces small movements of the wire at the tooltip of the torch synchronised with the current waveform in order to substantially reduce the heat input [8].

A basic WAAM system consists of an arc welding source, a positioning system (robot, 3/5-axis NC machines) and some additional and optional systems for controlling the process (e.g. active cooling, thermocamera, crack sensors). Differently from powder-based AM processes, WAAM allows a broad selection of filler material, base material, metal transfer mode, current waveform, heat treatments and deposition strategies. But the main advantage is related to the high deposition rate, as reported by Wu et al. [9]. The rate for GMAW standard transfer modes is about 3–4 kg/h; in tandem mode, it can reach 6–8 kg/h, while for cold metal transfer, CMT is about 2–3 kg/h. For processes that require lateral wire feed (rotation of the torch or the wire feed system) as gas tungsten arc welding (GTAW) and plasma arc welding (PAW), the deposition rates are about 1–2 kg/h and 2–4 kg/h, respectively. Both PAW and GTAW have an intrinsically lower fusion rate than GMAW. This is because in such processes the filler metal is not molten directly by the high temperature arc, but it is fed into the molten pool, which is at a lower temperature.

However, deposition rate is not the only topic to be addressed on WAAM; specimens with superior mechanical properties and workpiece weight were generated by Moradi et al. [10] in a modelling optimization of fused deposition study. A topological improvement using a CMT laser hybrid WAAM with a trailing laser beam was performed by Näsström et al. [11]. Wang et al. [12] evaluated the effect of single and double wire on the mechanical properties of an Al-Cu-Sn alloy deposited by WAAM, and the importance of the heat input in the forming and performance of depositions. The properties and the microstructure of an Al-Mg alloy fabricated by WAAM were studied by Ren et al. [13]. Yang et al. [14] using WAAM-CMT on AlSi7Mg0.6 thin-wall parts researched the effects of heat treatment on microstructure and mechanical properties. Prado-Cerqueira et al. [15] performed deposits with WAAM CMT using the steel wire AWS ER70S-6 to analyse mechanical and metallurgical properties. Different arc

modes were tested using WAAM CMT in 5183 aluminium alloy by Fang et al. [16]. Shassere et al. [17] developed a WAAM correction-based approach to improve bead geometrical conformity using the Surface Tension Transfer module depositing AWS ER70S-6 steel wire. Mechanical properties of AWS ER70S-6 steel wire deposited by WAAM were evaluated by Astarita et al. [18]. The effect of molten pool size on WAAM properties using Ti-6Al-4 V was studied by Wu et al. [19], finding that manufacturing parameters influence the cooling rate and thermal gradient and can control the equiaxial grain morphology formation. Another work about the grain refinement with GTAW applied to WAAM was made by Guo et al. [20] in a magnesium alloy by modifying the pulse frequency.

Martina et al. [21] studied the dilution values to different transfer modes and highlighted a strong influence of these since the value achieved for GMAW CMT is 3%, for GMAW pulsed AC is 8% and for GMAW pulsed+DC is 28%. A low dilution means preservation of the original substrate properties. Also, related to the toolpath planning, according to Geng et al. [22], the angle at which the filler metal is fed in the molten pool has a great influence on the bead geometry. Thus, the concentric wire feed in GMAW presents as a positive alternative to be applied in WAAM.

Another issue is how to maintain a stable arc reducing the heat input that requires a deep process control. Modifying the current waveform can reduce the heat transferred by the power source to the workpiece and avoid deleterious microstructural phases, distortion or thermal stresses. Currently, the state-of-the-art solutions are power sources able of achieving the controlled short-circuit current waveform. Norrish and Cuiuri [23] compared different controlled short-circuit power sources and CMT was identified as capable of combining low heat input, low spatter and equipment reliability. In the present work, to study the effect of some different deposition modes applied to WAAM, the following modes were selected: CMT, low spatter control (LSC) and pulsed synergic (PS).

Besides a particular waveform, CMT mode provides the wire motion control. LSC is a dip transfer arc with high arc stability and low level of spatter generation thanks to the adoption of an improved current waveform. The transfer process is based on short-circuit, the current is reduced before breaking the short-circuit bridge, leading to a soft reignition of the arc. Compared to GMAW short-circuit mode, the PS mode presents a lower heat transfer to the base metal resulting in less overall distortion and a reduction of some deleterious microstructures. In PS mode, the average current is reduced due the current pulse. In the lower period, the current pulse is kept at lower levels to not transfer the wire material, but high enough to not extinguish the electrical arc. Next, the peak current is raised above the transition current long enough to promote the formation and transfer of a metal drop. These known

deposition modes developed for fusion arc welding have been extensively used to WAAM.

The AISI H13 belongs to the hot-work steel group, martensitic chromium steel series and shows good strength and hardness at high temperatures. Some applications include the contact with other hot-work materials, as in die casting, extruding and hot forging, where the surface resistance to mechanic abrasive contact at high temperatures and mechanical resistance are required. The high temperature hardness properties are result of the moderate chromium content combined with carbide former elements, as molybdenum, vanadium and tungsten [24]. The hardness values generally range between 40 to 50 HRC [24]. Regarding the material AISI H13, one of the main issues is the cracking susceptibility. Recently, the number of studies focusing on additive manufacturing applications increased. In a study of H13 tools with nickel based (Stellite) electrodes, Rajeev et al. [25] using CMT deposited layers using different heat treatment conditions. It was found that cracking could be avoided by pre-heating and a post-weld annealing. Legesse et al. [26] used a hybrid CMT milling approach to manufacture an AISI H13 die. It showed that the workpiece could be manufactured avoiding cracks by using a pre-heating system. The deposition of H13 samples using a regular GMAW process was tried by Wang et al. [27], annealing was performed for 4 h at 830 °C and resulted, as expectable, in a significant reduction of the mechanical properties: tensile strength in the deposition direction decreased from 1085 to 536 MPa for the annealed ones. The deposition of a H13 free-crack block with limited porosity and proper mechanical properties using CMT was demonstrated to be possible by Ge et al. [28]; the material was deposited in an as-annealed substrate.

The main aim of this work is to analyse the effect of the above-mentioned deposition modes, characterised by lower heat inputs when compared to conventional GMAW, on the mechanical properties of AISI H13 tool steel applied to WAAM. The process parameters and the thermal history were analysed and related to the mechanical properties.

2 Experimental methods

To compare the influence of deposition mode in geometrical and mechanical characteristics of deposits produced using CMT, LSC and PS, a TPSi 320 CMT by Fronius® welding power source has been used. The CMT torch has been mounted on a 3-axis milling machine, whose numerical control could be programmed with standard ISO language to define and obtain the toolpath and the torch speed with good accuracy. The deposited beads were produced with the total

length of 170 mm and altering the deposition direction to avoid accumulation of material in the start point. The idle time for the depositions was set to 35 s. In general, idle times are used between the deposition of subsequent layers to allow reduction of the temperature under the phase transition range [29–32]. This value has been selected from preliminary tests in order to avoid an excessive remelting of the top layers and has been kept constant for all the tests. The wire feed material was a chromium-molybdenum-vanadium alloyed steel AISI H13 (EN X40CrMoV5-1) with diameter of 1.0 mm. According to the manufacturer Bohler-Uddeholm, this steel has a tensile strength of 1820 MPa and yield strength of 1520 MPa at room temperature when quench and tempered to achieve 52 HRC. Its chemical composition is indicated in Table 1. A carbon steel bar was used as base plate (substrate) for the depositions and had the dimensions of 250×150×12 mm. The substrate preheating was 120 °C.

The parameters set for all the depositions were the following: wire feed speed = 5.0 m/min; deposition speed = 240 mm/min; contact-tip-to-work-piece = 18 mm at first and the torch was moved 3.5 mm up after each deposit; shielding gas Ar + 2% CO₂ with 15 l/min flux; number of layers = 30. One deposition (wall) was performed for each type of deposition mode, and a general view of the deposits can be seen in Fig. 1.

Tensile tests specimens were machined in accordance with ASTM E8/E8M-16 [33] using the subsize dimensions with a 4 mm thickness, as can be observed in Fig. 2. For each wall, 3 tensile specimens were extracted longitudinally



Fig. 1 General view of deposits manufactured using the different deposition modes: CMT, LSC and PS

Table 1 Nominal chemical composition of AISI H13 steel wire (wt.%)

C	Cr	Mo	V	Mn	Si	Fe
0.39	5.3	1.3	0.9	0.4	1.0	Bal

to the building direction and named as “top”, “middle” and “base” with the purpose of verifying any possible influence of specimen position in results, since the bottom beads experience a larger number of thermal cycles than the top ones. The tensile tests were performed at room temperature on a universal testing machine (Instron MTS 810) with a constant speed of 0.5 mm/min.

Hardness and microstructural analysis were carried out in samples extracted from the grip section of each fractured tensile specimen, that is, transversally to the building direction, as shown in Fig. 1b, c. The samples have been mounted in phenolic resin and prepared using standard metallographic procedures: grinding in abrasive papers from 80# to 2000#-grit and polishing. The samples were etched with 2% Nital solution. Optical imaging was conducted using the microscope Nikon Eclipse LV150. The hardness Knoop has been performed using a Shimadzu HMV-2000 device using a load of 300 g and dwell time of 10 s. The distance between indentations was 0.5 mm, resulting in almost 20 hardness measurements in each specimen.

Thermal cycles were measured at substrate using K-type thermocouples. The position of the thermocouples is shown

in Fig. 3a; they were placed at distances of 5 mm (TC1 and TC2) and 12 mm (TC3) from the wall border (first bead). A resistance spot welding procedure was used to fix the thermocouples. An example of a complete deposit with thermocouples positioned is presented in Fig. 3b.

3 Results and discussion

The graphs of Fig. 4 show the measured deposition current and arc voltage for each layer of the three deposition modes. The deposition process parameters acquired using the integrated logger of power source are shown in Table 2 for each deposition mode. It is noteworthy to mention that, although the wire feed speed (W) has been set up as 5.0 m/min, internal control of the power source “adjusted” this value for each deposition mode, and the results are as indicated in Table 2. Moreover, the deposition energy input (E) for each deposition mode was calculated based on the mean arc power (IP) delivered by the source and the employed deposition speed, which was the same for the three deposition modes.

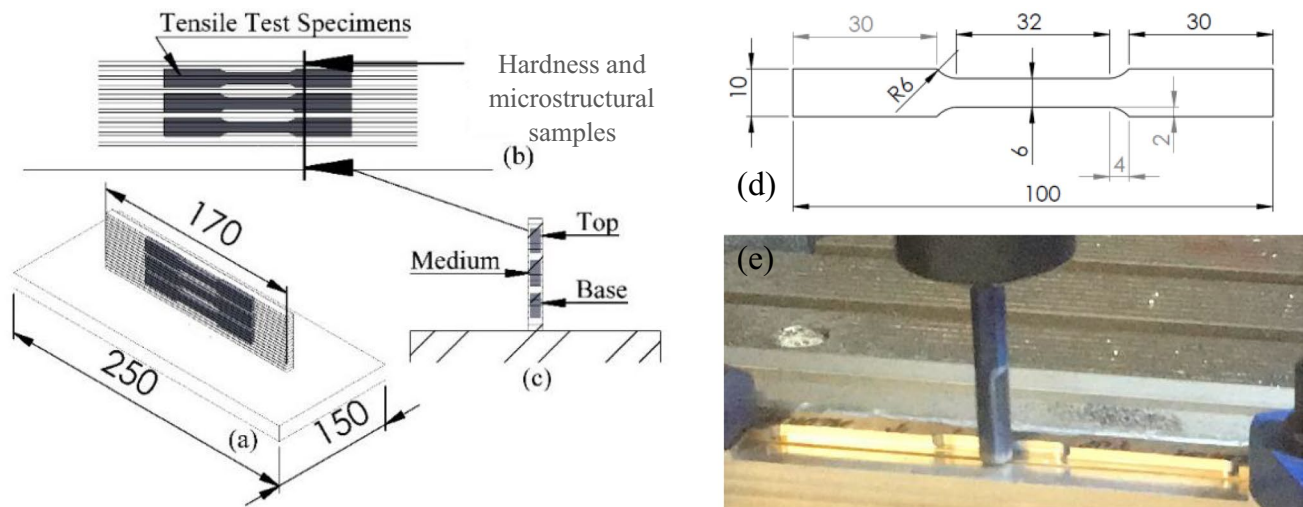
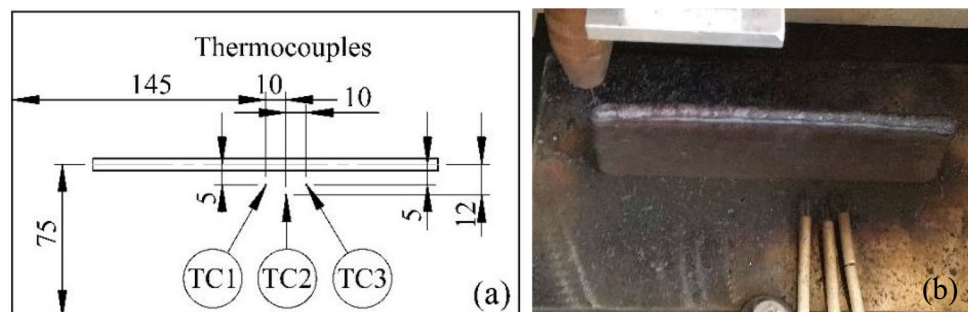


Fig. 2 a Schematic showing the dimensions of deposits and position of tensile test specimens. b, c Regions of micro-structural and hardness analysis. d Dimensions of tensile test specimens. e Specimen machining for tensile test

Fig. 3 a Schematic showing thermocouple positioning in substrate. b Example of a complete deposit with thermocouples in substrate



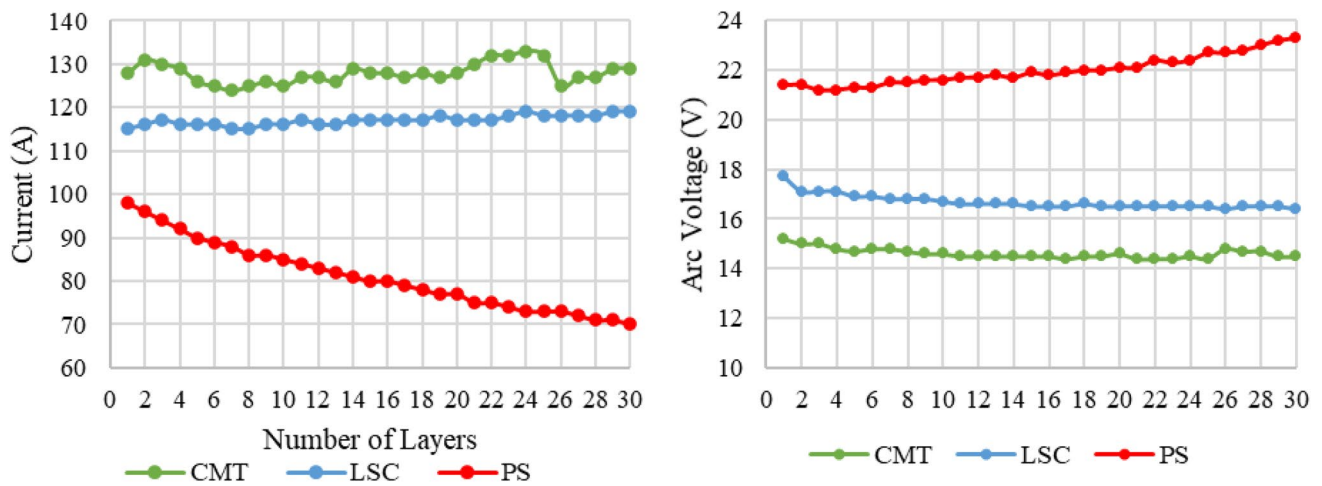


Fig. 4 Variations in electric current and arc voltage according to the deposited layer for each deposition mode

Table 2 Deposition parameters for CMT, LSC and PS deposition modes

	I (A)	U (V)	W (m/min)	IP (W)**	IE (kJ)***	E (kJ/cm)
CMT	128.0	14.5	5.8	2249	71.0	5.6
LSC	117.0	16.6	4.7	1914	65.0	4.8
PS	80.0	21.9	4.9	2153	62.0	5.4

Average values of 30 deposits
 **IP=mean value of arc power
 ***IE=total arc energy

Table 3 Geometries (height and width) for each deposition mode

	Height (mm)	Width (mm)
CMT	71.0	9.0
LSC	65.0	8.0
PS	62.0	8.3

In Fig. 4 can be observed small variations in deposition current and voltage for LSC. Although the higher dispersion of current values for CMT, and its higher current and lower voltage values compared to LSC, the same trend was noted for both deposition modes. However, the PS presented the lowest average current value and a decrease in its values as more layers were deposited; the difference from layer 1 to layer 30 was about 28.6%. The inverse trend was observed by the arc voltage in this mode, varying from 21.4 V in layer 1 to 23.3 in layer 30. The adopted deposition mode, and consequent parameters, affected the geometry of the deposits, as can be seen in Table 3 and Fig. 1. As stated before, the torch vertical movement between consecutive layers was kept constant (3.5 mm) to all deposits. As the total height of PS wall was the lowest, a small cumulative increase in the contact-tip-to-work distance (CTWD) should have produced the progressive increase in tension, compensated by synergic

power source programme by an electric current decrease. Also, the programme is generally designed for single pass and can be influenced by the heat accumulation as the part is build up [4]. Whereas the lower electric current value can be associated to the waveform and CTWD changes in PS, the higher current in CMT is related to the higher wire feed speed Table 2, which was adjusted by the source for this mode, leading to the highest deposition current between the three deposition modes. It is worth noting that, although the evident difference in deposition parameters, the resulting deposition energy input was similar for CMT and PS modes and slightly higher than that observed for the LSC.

The wall manufactured using CMT mode exhibited the larger height and was the widest. This can be attributed to the higher wire feed speed and deposition current, as the welding speed was the same for the three deposition modes. The electric current affects the deposition rate; there is an increase in wire fusion rate, and therefore deposition rate, with an increase in current. Even though the energy input for LSC was lower than that one for PS mode, its wall height was higher, again showing the significant effect of the electric current on deposition rate.

The increase in the heat input decreases the cooling rate, however, an increase in layer volume causes the opposite effect, facilitating the heat extraction. So, both the heat input

and deposition mode affect the manufactured deposits thermal cycles, as can be observed in Fig. 5. Although the thermocouple was placed in substrate, which implies in lower temperatures than that actual in the layer being deposited, it is possible to observe the general trend in thermal cycles for each deposition mode employed to produce the walls: the thermal cycles were more extenuated for LSC mode and sharper for PS mode. It is possible to note that even the pre-heating of substrate and the vicinity of thermocouple with the first layer, the peak temperatures were relatively low, reaching 255 °C, 271 °C and 353 °C for LSC, CMT and PS modes, respectively. This means that most of the heat generated during initial deposition was transferred to the base plate and to the surrounding environment (workbench, clamping system, ambient), as expected for these low energy deposition modes. Peak temperatures for each deposition mode are illustrated in Fig. 6. It is important to note that the thermocouple was not centralised to the total length of the deposit, so as the layers were produced in alternated deposition directions, when the deposition starts in the opposite

side of the point where the thermocouple is placed, it has more time to cool down until the heat source (torch) reaches the point again. This explains the alternating peak temperatures (as a “zig-zag”) when considering each thermal cycle (Fig. 5) or peak temperature (Fig. 6). LSC mode always presented the lowest peak temperature for each deposit, and this could be associated to its lowest deposition energy input compared to the other modes, as shown in Table 2. However, the energy input value per se is not capable to explain the difference in thermal cycle/peak temperature behaviours when comparing CMT and PS modes, because their energy input values were similar but peak temperatures observed for PS mode were higher than those for CMT mode, at least in the first deposited layers, where the minimum distance between to the thermocouple position is lower. The effect is due to the joint action of deposition current waveform and wire motion characteristic of CMT deposition mode.

The hardness profiles are shown in Fig. 7a, representing the total indentation points measured in samples extracted from tensile specimens, that is, in the vertical direction of

Fig. 5 Thermal cycles for CMT, LSC and PS deposition modes. Results referring to thermocouple 1 (TC1), placed in substrate at 5 mm from the border of the manufactured wall

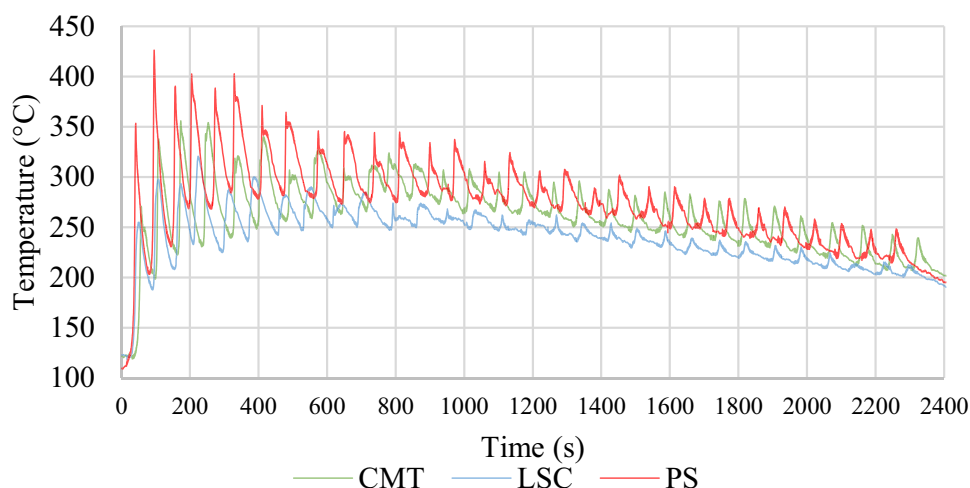
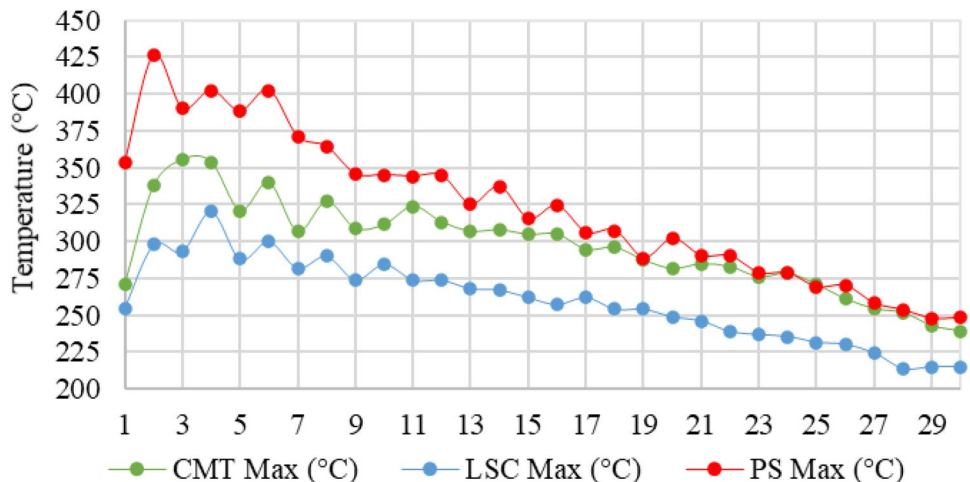


Fig. 6 Peak temperature for each layer for CMT, LSC and PS deposition modes. Data obtained from thermal cycles of Fig. 5



the deposition. Macrographic analysis were carried out and, although the heterogeneity in macrostructure, it was no observed internal defects (cracks, porosity, lack of fusion) in the manufactured walls. It was possible to note three different grain zones alternated between each layer are illustrated in Fig. 7b, c; these suggested zones (refined grain, partial refined grain, and coarse grain zones) are based on the common regions found in the heat affected zone in multipass welded joints [17, 34]. In general, it was noted that the lower values of hardness were found in the refined zone with prevalent equiaxial shape; the subsequent increase was related to the partial refined grain zone and finally the coarse grain zone, which presented larger columnar grains. For example, as shown in Fig. 7a, for the PS mode the indentation number 24 with 757 HK was performed in the coarse grain zone and the next one (indentation 25) with 746 HK referred to the refined zone. Then, these zones could be related to the hardness oscillation, Fig. 7a, in which new deposited layer creates new zones with specific microstructure due to the heating and cooling of the material. These mechanisms are common on additive manufacturing of metal parts, where the energy transferred by the power source and the cooling influence the final microstructure, and common for non-heat-treated WAAM deposits. That is, the hardness profile can support the representation of the heterogeneity of grain size and microstructure. It seems in Fig. 7a that the variation in hardness values is larger for PS deposition mode compared to the other ones, as well as smaller in the middle

specimens (approximately in the central region of wall height). As stated by Shassere et al. [17], the region with greater homogeneity in the hardness profile is also the one where the quasi-steady heat flow state is achieved.

Figure 8 indicates the average, minimum and maximum hardness values for each deposition mode according to the position in the vertical direction. A higher variation of hardness was observed in the regions near the substrate and in the top layers: the lowest hardness value of 690 HK (approximately 58 HRC) was observed in a base sample for the PS deposition mode, whereas the maximum of 826 HK (near 64 HRC) occurred for both CMT and PS modes, in a base and a top sample, respectively. The overall results shown in Fig. 7 and Fig. 9 indicate that, even considering the lowest hardness result, these values are very high and indicative of a microstructure composed by hard phases. The AISI H13 is a carbon steel alloyed with chromium, molybdenum and vanadium, which are strong carbide formers. This steel has high hardenability, and transformation of austenite into martensite occurs for a wide range of cooling rates. It means that the deposition modes employed and subsequent thermal cycles did not cause significant alterations in the hardness values of the AISI H13 steel deposits.

The results of tensile tests are presented in Fig. 9, where is also possible to observe the individual results for base, middle and top samples for each deposition mode. The strength values are high, however inferior to the one specified by the manufacturer using conventional routes of fabrication.

Fig. 7 a Hardness profile for CMT, LSC and PS deposition mode. b Macrograph of CMT top specimen, indentation 13–755 HK. c Macrograph of LSC medium specimen, indentation 17–756 HK. The three macroregions are highlighted (coarsening, partial and refining grain zones)

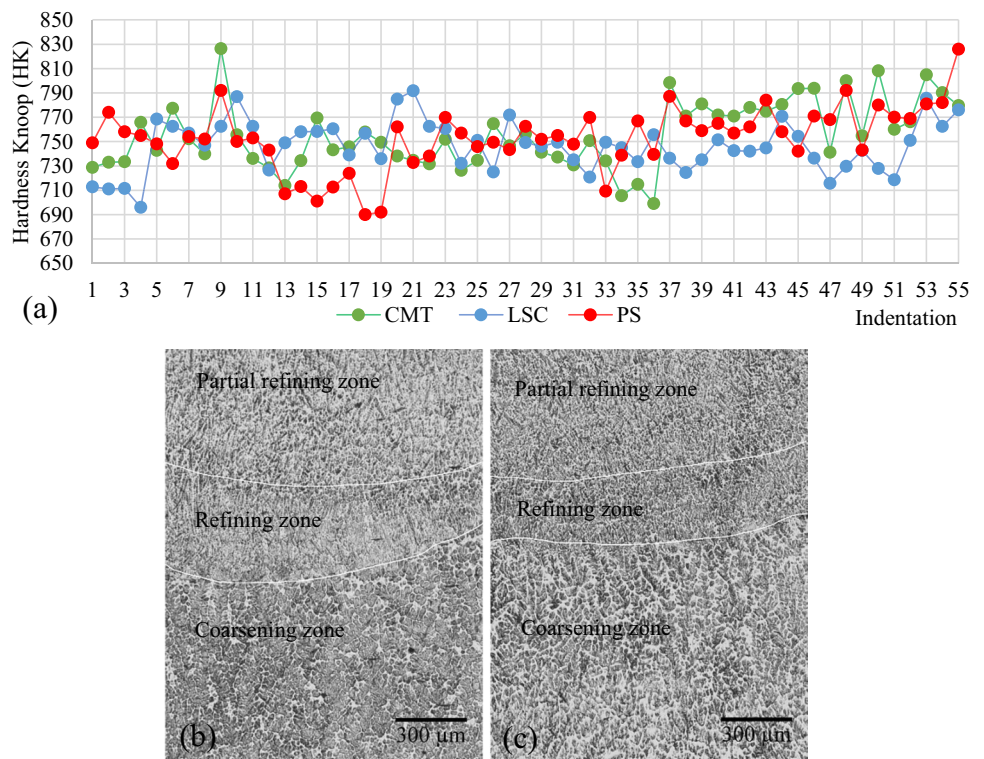


Fig. 8 Hardness results for the base, middle and top samples for CMT, LSC and PS deposition mode

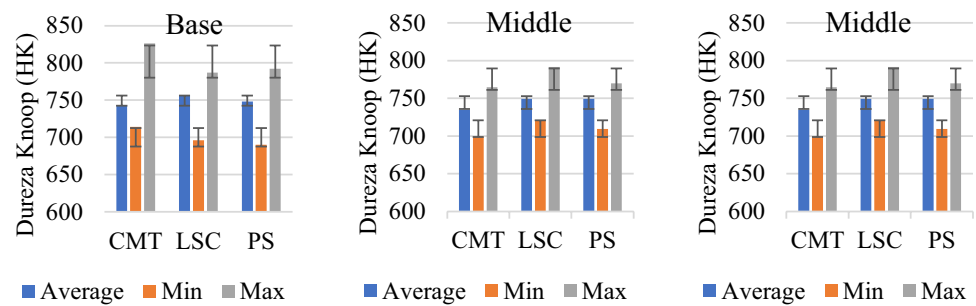
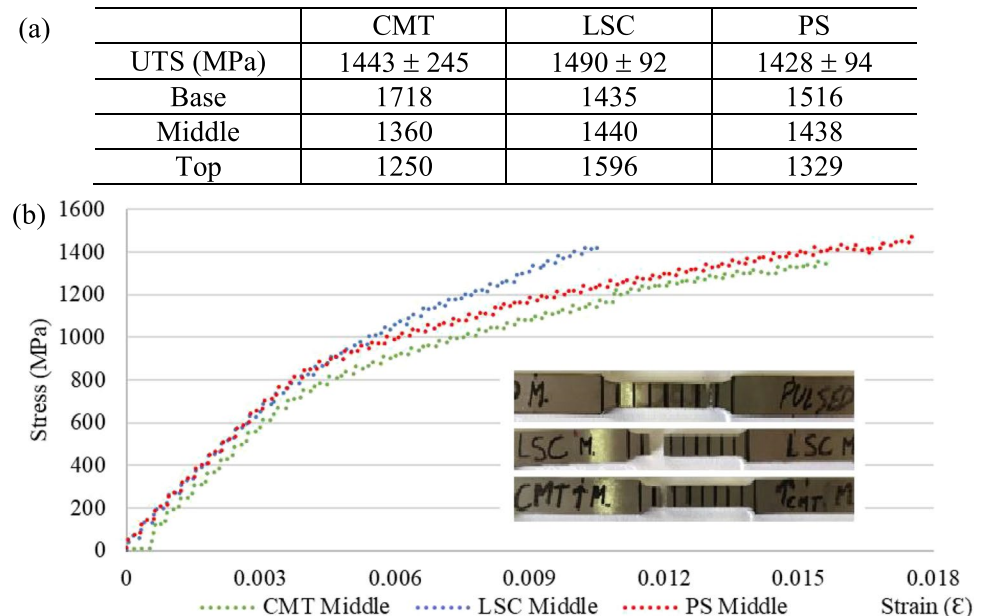


Fig. 9 Results of tensile tests for each deposition mode. **a** Average and individual values. **b** Example of stress–strain curve and fractured specimens extracted from the middle region of the manufactured wall



The specimens did not present the necking, with a brittle fracture, as can be seen in the example in Fig. 9b, the low elongation preventing the attainment of full tensile strength. Besides, considering the dispersion in results, it was not observed significant difference between them related to the deposition modes. There are some factors that could contribute to the unsatisfactory mechanical properties. Residual stresses can affect mechanical properties. They originate from gradient temperatures during deposition process as well as from the cooling-down and from solid-state phase transformations [35]. Cottam et al. [36] used direct metal deposition to produce a part of AISI H13 steel and demonstrated that transformation of retained austenite to martensite caused compressive stress regions, whereas regions of tensile stress were attributed to the martensite being tempered by the heat from the laser during building-up. Besides, it was demonstrated that the distribution of stress was not symmetrical [36]. In the present study, residual stresses were not evaluated, but thermal gradients are inherent to the WAAM, and solid phase transformations are characteristic to the AISI H13. Another point that could contribute to the strength results is the heterogeneity in grain structure caused

by regions with equiaxial, columnar and dendritic grains, which during tension behave in different ways and therefore can cause a non-homogeneous deformation, creating zones with stress concentration. At last, the properties of the highly alloyed AISI H13 are very dependent of the schedule and parameters applied during heat treatment. The deposition modes used in this study induced several thermal cycles in the material, which in its turn induced to “not controlled” microstructural alterations. In fact, as stated bellow, the resulting deposition microstructures had a major influence on the mechanical properties.

According to Ning et al. [37], in usual heat treatment processing routes for AISI H13 steel, most of carbides dissolve in quenching temperatures, and there is a precipitation stage during tempering, forming nanoparticles. The tempering schedule typically uses two-step tempering to transform any residual retained austenite into martensite. Lerchbacher [38] cites that typical precipitation sites for alloyed carbides in tool steels includes dislocations, previous carbides (as cementite) and boundaries of formed austenite and martensite laths. Quenching temperature affects the austenite grain size and, consequently, lath width of

martensite. Therefore, the size and distribution of the precipitates, as well as martensite lath width and amounts of retained austenite, affect the toughness and strength of the AISI H13 steel.

The highly alloyed AISI H13 steel provides martensitic structure at relatively low cooling rates and its carbides are rich in vanadium, chromium and molybdenum. Figure 10 shows that all microstructures were composed by a matrix of martensite and carbides precipitated in the matrix and in grain boundaries, along with retained austenite. It is possible to note in Fig. 10 that the martensite had the lath morphology; however, it seemed more tempered when the CMT deposition mode was employed. Regarding to the retained austenite, the high amount of alloying elements in AISI H13 steel facilitates segregation during solidification, which generally occurs in intercellular or interdendritic regions. The segregation can contribute in some cases to hot cracking but also can stabilise (chemically) the austenite, lowering the martensite-start temperature (M_s), because there is a dependence of M_s with the chemical composition of austenite.

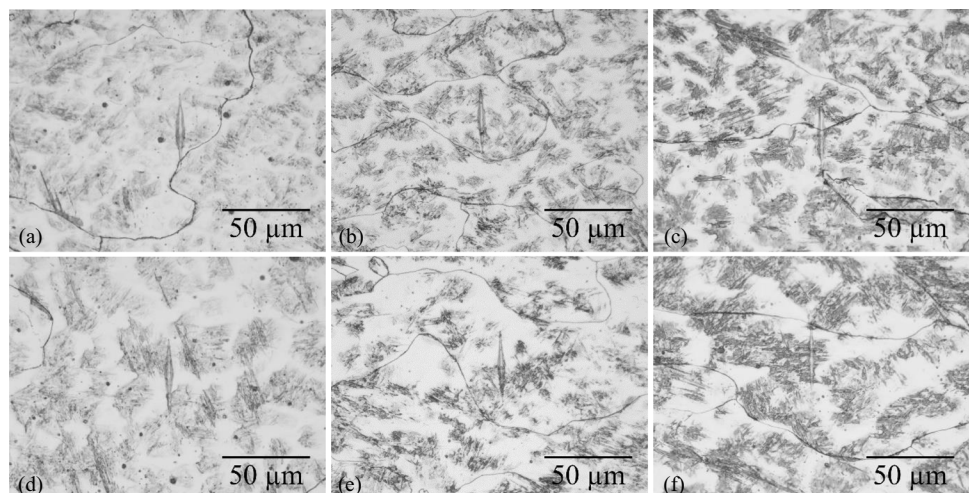
During the building-up of the walls, the martensitic structure was partly tempered due to the re-heating when a new layer was deposited. Also, the repetitive thermal flow facilitated the diffusion of alloying elements, leading to a coarsening of the precipitates. In Fig. 10, it is possible to note that precipitates using the CMT mode were more visible and larger than the ones observed in LSC and PS deposition modes. However, as already cited, for all deposition modes employed, it was observed precipitation in grain boundaries. Therefore, the embrittlement of tensile specimens can be attributed to stress concentration generated in these regions during tension.

4 Conclusions

In this work was studied the effect of deposition modes as cold metal transfer (CMT), low spatter control (LSC) and pulsed synergic (PS) applied to WAAM process on the mechanical properties and thermal cycles of AISI H13 steel. Based on the experimental results and the analyses, the following conclusion can be stated:

- The additive manufacturing via WAAM applied to AISI H13 steel proved to be viable with the different modes of metal transfer, CMT, LSC and PS. All deposition modes produced deposits without discontinuities.
- Regarding the electric deposition parameters, the LSC and CMT modes exhibited similar mean values of arc voltage and current, while the PS mode presented oscillations during the consecutive deposition layers resulting in the lower arc current and higher voltage mean values. The lowest energy was observed for LSC mode. The PS mode exhibited the highest substrate temperatures, but its volume of deposited metal was the lowest. CMT mode produced the tallest and widest deposit wall.
- Comparing the three deposition modes studied in this work, no strong differences were found in the mechanical properties evaluated. The hardness results were very high indicating the presence of hard phases in the microstructure. High tensile strength values were obtained, but all the specimens exhibited low elongation brittle fracture. The microstructure was composed by martensite, carbides and retained austenite. Grain boundary precipitates caused the embrittlement observed in tensile tests.
- According to the remarks above, although the three deposition modes studied, CMT, LSC and PS, allow to achieve WAAM deposits exhibiting similar characteristics, the mechanical properties of the deposits were not

Fig. 10 Microstructures observed in grain refined zones (a–c) and coarse grain zones (d–f). **a** CMT 28–756 HK. **b** LSC 10–746 HK. **c** PS 10–752 HK. **d** CMT 27–747 HK. **e** LSC 11–749 HK. **f** PS 12–748 HK. All the images belong to middle samples. Numbering refers to the hardness indentation and value measured



satisfactory because of the metallurgical characteristics of the AISI H13 steel. Another deposition schedule or application of a heat treatment could improve the properties of deposits.

Acknowledgements The author William Hackenhaar would like to acknowledge the support by the Brazilian research agency, Coordination for the Improvement of Higher Education Personnel (CAPES)—PDSE [88881.189938/2018-01].

Funding This research has received funding from the European Union's Horizon 2020 research and innovation programme under grant agreement n° 721267 through ManuNet initiative—RetroFix project.

Data availability The data that support the findings of this study are available from the corresponding author upon a reasonable request.

Declarations

Conflicts of interest The authors declare no competing interests.

References

- Wohlers T, Kowen J, Diegel O, Campbell I (2018) Wohlers Report 2018: 3D printing and additive manufacturing state of the industry: Annual Worldwide Progress Report
- Xu X (2017) Machine Tool 4.0 for the new era of manufacturing. *Int J Adv Manuf Technol* 92:1893–1900. <https://doi.org/10.1007/s00170-017-0300-7>
- Petch M (2020) 3D printing community responds to COVID-19 and coronavirus resources. <https://3dprintingindustry.com/news/3d-printing-community-responds-to-covid-19-and-coronavirus-resources-169143/>. Accessed 19 May 2020
- Cunningham CR, Flynn JM, Shokrani A et al (2018) Invited review article: Strategies and processes for high quality wire arc additive manufacturing. *Addit Manuf* 22:672–686. <https://doi.org/10.1016/j.addma.2018.06.020>
- RAMLAB (2017) World's first class approved 3D printed ship's propeller. <https://ramlab.com/updates/ramlab-unveils-worlds-first-class-approved-3d-printed-ships-propeller/>. Accessed 21 May 2020
- Williams SW, Martina F, Addison AC et al (2016) Wire + arc additive manufacturing. *Mater Sci Technol* 32:641–647. <https://doi.org/10.1179/1743284715Y.0000000073>
- MAZAK Corporation (2020) Hybrid multi-tasking machine INTEGEX i-400 AM (additive manufacturing). <https://www.mazakusa.com/machines/integrex-i-400am/>. Accessed 19 May 2020
- Fronius International GmbH. (2014) Cold Metal transfer: the technology. www.fronius.com. Accessed 12 Oct 2016
- Wu B, Pan Z, Ding D et al (2018) A review of the wire arc additive manufacturing of metals: properties, defects and quality improvement. *J Manuf Process* 35:127–139
- Moradi M, Meiabadi S, Kaplan A (2019) 3D printed parts with honeycomb internal pattern by fused deposition modelling; experimental characterization and production optimization. *Met Mater Int* 25:1312–1325. <https://doi.org/10.1007/s12540-019-00272-9>
- Näsström J, Brueckner F, Kaplan AFH (2019) Laser enhancement of wire arc additive manufacturing. *J Laser Appl* 31:022307. <https://doi.org/10.2351/1.5096111>
- Wang S, Gu H, Wang W et al (2019) Study on microstructural and mechanical properties of an Al–Cu–Sn alloy wall deposited by double-wire arc additive manufacturing process. *Materials (Basel)* 13:73. <https://doi.org/10.3390/ma13010073>
- Ren L, Gu H, Wang W et al (2019) Effect of Mg content on microstructure and properties of Al–Mg alloy produced by the wire arc additive manufacturing method. *Materials (Basel)* 12:4160. <https://doi.org/10.3390/ma12244160>
- Yang Q, Xia C, Deng Y, et al (2019) Microstructure and mechanical properties of AlSi7Mg0.6 aluminum alloy fabricated by wire and arc additive manufacturing based on cold metal transfer (WAAM-CMT). *Materials (Basel)* 12:. <https://doi.org/10.3390/ma12162525>
- Prado-Cerqueira JL, Camacho AM, Diéguez JL et al (2018) Analysis of favorable process conditions for the manufacturing of thin-wall pieces of mild steel obtained by wire and arc additive manufacturing (WAAM). *Materials (Basel)* 11:1449. <https://doi.org/10.3390/ma11081449>
- Fang X, Zhang L, Chen G et al (2018) Correlations between microstructure characteristics and mechanical properties in 5183 aluminium alloy fabricated by wire-arc additive manufacturing with different arc modes. *Materials (Basel)* 11:2075. <https://doi.org/10.3390/ma11112075>
- Shassere B, Nycz A, Noakes MW, et al (2019) Correlation of microstructure and mechanical properties of Metal Big Area Additive Manufacturing. *Appl Sci* 9<https://doi.org/10.3390/app9040787>
- Astarita A, Campatelli G, Corigliano P, Epasto G (2019) Microstructure and mechanical properties of specimens produced using the wire-arc additive manufacturing process. 0:1–11<https://doi.org/10.1177/0954406219883324>
- Wu Q, Lu J, Liu C et al (2017) Effect of molten pool size on microstructure and tensile properties of wire arc additive manufacturing of Ti-6Al-4V alloy. *Materials (Basel)* 10:1–11. <https://doi.org/10.3390/ma10070749>
- Guo J, Zhou Y, Liu C, et al (2016) Wire arc additive manufacturing of AZ31 magnesium alloy: grain refinement by adjusting pulse frequency. *Materials (Basel)* 9<https://doi.org/10.3390/ma9100823>
- Martina F, Ding J, Williams S et al (2019) Tandem metal inert gas process for high productivity wire arc additive manufacturing in stainless steel. *Addit Manuf* 25:545–550. <https://doi.org/10.1016/j.addma.2018.11.022>
- Geng H, Li J, Xiong J et al (2017) Optimization of wire feed for GTAW based additive manufacturing. *J Mater Process Technol* 243:40–47. <https://doi.org/10.1016/j.jmatprotec.2016.11.027>
- Norrish J, Cuiuri D (2014) The controlled short circuit GMAW process: a tutorial. *J Manuf Process* 16:86–92. <https://doi.org/10.1016/j.jmapro.2013.08.006>
- AWS (1991) *Welding Handbook - Materials and Applications*. American Welding Society
- Kamaraj GPRM, Bakshi SR (2017) Hardfacing of AISI H13 tool steel with Stellite 21 alloy using cold metal transfer welding process. *Surf Coatings Technol* 326:63–71. <https://doi.org/10.1016/j.surfcoat.2017.07.050>
- Legesse F, Kapil S, Vithasth H, Karunakaran KP (2018) Additive manufacturing of H13 tooling element with conformal cooling channel using MIG cladding. *Int J Rapid Manuf* 7:1. <https://doi.org/10.1504/IJRAPIDM.2018.089725>
- Wang X, Wang J, Gao Z et al (2018) Fabrication of graded surfacing layer for the repair of failed H13 mandrel using submerged arc welding technology. *J Mater Process Technol* 262:182–188. <https://doi.org/10.1016/j.jmatprotec.2018.06.040>
- Ge J, Ma T, Chen Y et al (2019) Wire-arc additive manufacturing H13 part: 3D pore distribution, microstructural evolution, and mechanical performances. *J Alloys Compd* 783:145–155. <https://doi.org/10.1016/j.jallcom.2018.12.274>

29. Gou J, Shen J, Hu S et al (2019) Microstructure and mechanical properties of as-built and heat-treated Ti-6Al-4V alloy prepared by cold metal transfer additive manufacturing. *J Manuf Process* 42:41–50. <https://doi.org/10.1016/j.jmapro.2019.04.012>
30. Montevecchi F, Venturini G, Grossi N et al (2018) Idle time selection for wire-arc additive manufacturing: a finite element-based technique. *Addit Manuf* 21:479–486. <https://doi.org/10.1016/j.addma.2018.01.007>
31. Lei Y, Xiong J, Li R (2018) Effect of inter layer idle time on thermal behavior for multi-layer single-pass thin-walled parts in GMAW-based additive manufacturing. *Int J Adv Manuf Technol* 96:1355–1365. <https://doi.org/10.1007/s00170-018-1699-1>
32. Hackenhaar W, Mazzaferro JAE, Montevecchi F, Campatelli G (2020) An experimental-numerical study of active cooling in wire arc additive manufacturing. *J Manuf Process* 52:58–65. <https://doi.org/10.1016/j.jmapro.2020.01.051>
33. ASTM (2016) ASTM E8/E8M. standard test methods for tension testing of metallic materials. 29
34. Kou S (2002) *Welding metallurgy*
35. Chen H, Gao Y, Zhang Q, Wu Z, Gao XZ (2022) Review on residual stresses in metal additive manufacturing: formation mechanisms, parameter dependencies, prediction and control approaches. *J Mater Res Technol* 17:2950–2974
36. Cottam RJW (2014) Characterization of microstructure and residual stress in a 3D H13 tool steel component produced by additive manufacturing. *J Mater Res* 29:1978–1986. <https://doi.org/10.1557/jmr.2014.190>
37. A. Ning, W. Mao, X. Chen, H. Guo JG (2017) Precipitation behavior of carbides in H13 hot work die steel and its strengthening during tempering. *Metals (Basel)* 7 <https://doi.org/10.3390/met7030070>
38. Lerchbacher C (2013) The effect of cooling rate on the microstructure and its influence on toughness of two types of tool steels studied by high resolution techniques. University of Leoben

Publisher's note Springer Nature remains neutral with regard to jurisdictional claims in published maps and institutional affiliations.